Robust control strategy for PV system integration in distribution systems

Robust Control Strategy for PV System Integration in Distribution Systems

M. J. Hossain[1], T. K. Saha[2], N. Mithulananthan[2] and H. R. Pota[3]

[1] Griffith School of Engineering, Griffith University, Gold Coast, QLD 4022, Australia

Tel. +61432155461, e-mail: j.hossain@griffith.edu.com.

[2] School of ITEE, The University of Queensland, Brisbane, QLD 4072, Australia

Tel. +61733653962, e-mail: m.hossain9@uq.edu.com,

saha@itee.uq.edu.au, mithulan@itee.uq.edu.au.

[3]SEIT, The University of New South Wales, Canberra, ACT 2600, Australia

Tel. +61262688197, email: h.pota@adfa.edu.au.

Abstract This paper proposes a decentralized control strategy for higher penetration of photovoltaic (PV) units without violating system operating constraints. A systematic procedure is developed and a robust controller is designed to ensure both dynamic voltage and transient stability for a specific PV integration level. The change in the model due to the volatile nature of PV generations is considered as an uncertain term in the design algorithm. Simultaneous output-feedback linear quadratic controllers are designed for PV generators. This designed control scheme is robust with respect to intermittency and enhances the integration level in a sub-transmission and distributed system. The effectiveness of the proposed controller is verified on a 43-bus industrial meshed distribution system under large disturbances. It is found that the designed control scheme enhances stability and increases the renewable integration levels.

Key Words -- Distributed Generation, Photovoltaic (PV) Generators, Voltage Constraints, Decentralized Control, and Generation and Load Uncertainties

1. Nomenclature

PV	Photovoltaic
DG	Distributed generation
PI	Proportional integral
I_{ON}	Dark diode characteristics of photocells
I_L	Light-generated current
L_{pv}, C_{pv}	Wiring inductance and capacitance of PV
I_s	Saturation current
R_s, R_{sh}	Series and shunt resistances
α	Firing angle of PWM scheme
K	Amplitude modulation index
i_{pv}	Current flowing through array
v_{pv}	Output voltage of array
R_{dc}, L_{dc}, C_{dc}	Resistance, reactance and capacitance of DC-link
i_{dc}	Current flowing through DC-link
R_{out}, L_{out}	Resistance and reactance of line connected to grid
i_{out}	Current flowing through line connected to grid
q	Charge of electron
T	Temperature
x	State vector
u	Control input
y	Measured output
ζ	Uncertainty output

ξ	Uncertainty input
A, B, C, D	System matrices
τ, θ	Free parameters

2. Introduction

The installed capacity of distributed generation (DG) using a wide range of technologies is expected to continue to increase over the coming years [1, 2]. The technologies of DG include PV generators, wind turbines, small hydro turbines, combined heat and power (CHP) units and fuel cells. Due to this wide variety of technologies, the integration of small, decentralized power generators into medium and low-voltage power grids brings technical challenges which have to be resolved in order to obtain benefits from the interconnection of wide-scale DG units to existing grids. Of the existing DG units, PV is becoming increasingly attractive in certain countries due to the availability of resources and environmental benefits [3]. PV systems are connected primarily to the power systems at sub-transmission voltage levels; however, it is expected they will be increasingly connected to distribution networks in near future [4]. The large-scale integration of PV generators into sub-transmission and distribution grids can have a significant impact on a power system's operation and stability [5, 6].

It is well known that a sudden change in sunlight can initiate a rapid disconnection or reduction in a PV generating capacity. As the penetration of PV schemes increases, this can lead to a problem of voltage variation and transient voltage instability in the case of a weak coupling with the grid [6]. The large-scale penetration of PV units also has an impact on the short-term voltage and transient stability of a system, which is not only restricted to the distribution network but begins to influence the whole system [7].

Therefore, it is significantly important to control the output power to ensure stability and security. The implementation of appropriate controls for PV units can improve the system's performance without violating network constraints and can facilitate the effective participation of PV penetration.

Different control systems for accommodating PV units in a network are currently being investigated. The optimum power flow technique has been used for distribution systems with a few DG units [8], [9]. A new voltage control procedure that includes a series reactor is proposed in [10]. The authors in [11] present a frequency control for smoothing the PV power output fluctuation using fuzzy logic control. Another droop control approach for frequency control using a capacitor is discussed in [12]. Most of these approaches use centralized control techniques, which need the global transmission of signals. However, this type of control is expensive for a geographically dispersed distributed system, which makes it difficult to ensure the resulting system is robust [13].

In a distributed system, decentralized control modes, such as maximum power point tracking control [14], voltage and frequency control [15, 16] and feeder power flow control [17, 18], are applied. However, the fact that such a controller cannot stabilize a system for severe large disturbances motivates the use of advanced control techniques, which consider nonlinear interactions and ensure stability under large disturbances [19, 20].

This paper presents a new decentralized controller for robust PV integration that ensures stability during large disturbances and large swings in PV outputs without violating grid codes and system constraints. In the system model, changes in PV outputs are considered with uncertainty and the controller is synthesized via optimization of the worst-case quadratic performance of the underlying uncertain system. In addition, the

interconnection effects of other PV systems are considered in the controller design, which enhance the robustness of the closed loop system. The designed controller guarantees stability under changing conditions as compared to, for example, most PI controllers which are tuned for a few operating conditions and then tested using simulations.

The organization of this paper is as follows: the notation and symbols used throughout it are listed in Section 1, and Section 2 explains the motivation and current state-of-the-art approaches to the control of PV units. Section 3 provides the mathematical modeling of a distribution system, including PV generators. The test system and control objectives are presented in Section 4. Section 5 describes the decentralized output-feedback controller design procedure and Section 6 depicts the control design algorithm. The performance of the controller is demonstrated through a series of nonlinear simulations and the results are presented in Section 7. Concluding remarks and suggestions for future work are given in Section 8.

3. System modelling

As shown in Figure 1 PV plants have mainly two parts, (i) solar conversion and (ii) electrical interface with the electrical network (power electronic converter). The power converters are supplied from PV sources that convert the sun irradiance energy to DC power. A PV array system is connected to the grid through a DC-DC converter and a DC-AC inverter. A DC-DC converter serves the purpose of transferring maximum power from the solar module to the load. The equivalent model of a grid-connected PV system [21, 22] consisting of several switching elements is shown in Figure 2. As it is very difficult to fully model a PV system for stability analysis, due to the nonlinear nature of the switching schemes, ideal switching devices are considered here [23]. A

step-up transformer with a turns-ratio (N) is connected to increase the voltage level of the PV array. Although the output of the inverter is not purely sinusoidal, it is considered to be sinusoidal in [24].

<Figure 1>

Figure 1. PV system connected to grid.

The equivalent circuit, with the approximations previously mentioned, is shown in Figure 3 in which I_L is the light-generated current, I_{ON} the dark diode characteristics of the photocells, L_{pv} and C_{pv} the wiring inductance and capacitance of the PV cells, respectively, $I_s = 9 \times 10^{-11}$ the saturation current, R_s and R_{sh} the series and shunt resistances of the array, respectively, δ the firing angle, K the amplitude modulation index of the pulse-width modulation (PWM) scheme, i_{pv} the current flowing through the array, v_{pv} the output voltage of the array, R_{dc} the resistance of, L_{dc} the reactance of, C_{dc} the capacitance of, i_{dc} the current flowing through and, v_{dc} the output voltage of the DC link, R_{out} and L_{out} the resistance and reactance of the line connected to the grid, respectively, i_{out} the current flowing through the line connected to the grid, and $v_g = V_g \cos(\omega t)$ the AC voltage of the grid where V_g is the magnitude of v_g.

<Figure 2>

Figure 2. Equivalent model of grid-connected PV system.

<Figure 3>

Figure 3. Equivalent circuit diagram of grid-connected PV system.

Now, by applying KCL in the PV terminals, we get:

$$I_L - I_S[\exp[\alpha(v_{pv} + R_s i_{pv} + L_{pv} + \frac{di_{pv}}{dt})] - 1] - \frac{v_{pv} + R_s i_{pv} + L_{pv} \frac{di_{pv}}{dt}}{R_{sh}} - i_{pv} = 0 \quad (1)$$

where $\alpha = \frac{q}{nskT}$, $k = 1.3807 \times 10^{-23}\ JK^{-1}$ is the Boltzmann's constant, $q = 1.6022 \times 10^{-19}\ C$ the charge of electron, *T*=298 *K* the temperature and *ns* the number of series cells in the PV array. Since the values of L_{pv} and $1/R_{sh}$ are very small, we can neglect the terms (L_{pv}/R_{sh}) and (di_{pv}/dt) in the above equation and write:

$$\frac{di_{pv}}{dt} = \frac{1}{\alpha L_{pv}} \ln\left(\frac{I_L - i_{pv} - \frac{v_{pv} + R_s i_{pv}}{R_{sh}}}{I_s}\right) - \frac{1}{L_{pv}}(v_{pv} + R_s i_{pv}) \quad (2)$$

Then, by applying KCL at the PV capacitor, we get:

$$\frac{dv_{pv}}{dt} = \frac{1}{C_{pv}}[i_{pv} - N i_{dc}] \quad (3)$$

In a similar way, KCL at the DC link results in:

$$\frac{di_{dc}}{dt} = \frac{1}{L_{dc}}[N v_{pv} - R_{dc} i_{dc} - v_{dc}] \quad (4)$$

The DC link voltage dynamics can be given based on the principle of power balance

$$\frac{d}{dt}\left(\frac{1}{2} C_{dc} v_{dc}^2\right) = P_{pv} - P \quad (5)$$

$v_{td} = v_{dc} k_{vdc} m_{td}$, $v_{tq} = v_{dc} k_{vdc} m_{tq}$, where $P = \frac{3}{2}(v_{td} i_{td} + v_{tq} i_{tq})$, $P_{pv} = f(v_{dc}, G, T)$,

k_{vdc} is 0.5 for carrier based sinusoidal PWM [24].

Finally, the average model of the voltage source converter (VSC) as shown in Figure 2 is given

$$P_{dc} = P_{ac} \quad (6)$$

4. Test system and control strategy

A 43-bus industrial meshed system is used in this paper [25]. A single-line diagram of it is shown in Figure 4 and the numerical values of its parameters are given

in Appendix I. The PV generators are connected at buses 4, 50 and 39. There are five different voltages levels in this test distribution system: 69kV, 13.8kV, 4.16kV, 2.4kV and 0.48kV. In the original system, the two plant generators at buses 4 and 50 supply 87% of the real power load, with the remainder coming from the main grid through the substation located at bus 100. This is a meshed distribution system with a total load of 21.76 MW and 9 MVAr which is made up of (i) an 80% induction motor load [20] and (ii) a 20% static load. The dynamic model of induction motors as given in [20] is used for simulations. To study this, the test system is stressed by increasing both the generation and the load demand to twice that given in [25].

<Figure 4>

Figure 4. Single-line diagram of 43-bus test distribution system.

The test system considered in the research work is divided into three subsystems based on the coherent groups (generators swing together) of generating units: (i) Bus 4, PV system 1, (ii) Bus 50, PV system 2 and (iii) Bus 39, PV system 3. In this paper, a decentralized control for the inverter to enhance PV integration into the grid is designed. The proposed inverter control strategy is shown in Figure 5. In the voltage control mode of PV, P and Q are controlled by the amplitude of the VSC terminal voltage. The error signals P_{refi}-P_i and Q_{refi}-Q_i are fed to the controller which produces d- and q-axis components of the VSC terminal voltage. These two signals are then divided by the VSC amplification gain $k_{vdc}v_{dc}$ to generate m_{td} and m_{tq} for the pulse width modulation (PWM). Real power reference for the proposed control is determined by the maximum power point control [23] and reactive power reference from the steady state solution and then the designed control is used to regulate P_{refi} and Q_{refi}. The measured feedback signal as shown in Figure 5 for the controller is $y_i=[P_i \quad Q_i]$ and control input $u_i=[m_{tdi} \quad m_{tqi}]$.

<Figure 5>

Figure 5. Control strategy for PV.

5. Problem formulation

The power system model used in this paper is described by the following large-scale system comprising N subsystems denoted by S_i, i=1,2, . . .N [26-28]:

$$S_i : \dot{x}(t) = A_i x_x(t) + B_i u_i(t) + E_i \xi_i(t) + L_i r(t) \quad [7]$$

$$z_i(t) = C_i x_x(t) + D_i \xi_i(t) \quad [8]$$

$$\zeta_i(t) = G_i x_x(t) + H_i u_i(t) \quad [9]$$

$$y_i(t) = C_{yi} x_x(t) + D_{yi} \xi_i(t) \quad [10]$$

where $x_i \in R^{ni}$ is the state vector, $u_i \in R^{mi}$ the control input, $\xi_i \in R^{pi}$ the perturbation, $\zeta_i \in R^{hi}$ the uncertainty output, $z_i \in R^{qi}$ the controlled output, $y_i \in R^{gi}$ the measured output, and the input r_i describes the effect of the other subsystems (S_1, . . . , S_{i-1}, s_{i+1}, . . . , S_N) on subsystem S_i. The structure of this system is shown in Figure 6. For each subsystem chosen in this paper: $x_i = [i_{pvi} \;\; v_{pvi} \;\; i_{dci} \;\; v_{dci}]^T$, $u_i = [m_{tdi} \;\; m_{tqi}]^T$ and $y_i = z_i = [P_{gi} \;\; Q_{gi}]$.

<Figure 6>

Figure 6. Block diagram of decentralized control.

Equations (7) to (10) represent a generic interconnected uncertain system in which each subsystem is affected by two types of uncertainties, one local and other due to system interconnections.. In this paper, the local uncertainties arise from the change in the linearized subsystem model due to the changes in solar generation levels. Such

dynamics is driven by the uncertainty output (ζ_i) of subsystem S_i. A second source of uncertainty arises from interactions among the subsystems of the large-scale system. The proposed decentralised robust controller design includes interconnection terms as modelling uncertainty.

In the design process three common assumptions are made: (i) $D_i^T D_i + G_i^T G_i > 0$ and $D_{yi} D_{yi}^T > 0$; (ii) the pair $(A_i, C_i^T C_i)$ is observable; and (iii) the pair $(A_i, B_i^T B_i)$ is able to be stabilized. It can be easily verified that the system under consideration satisfied these assumptions.

We define $\zeta_i = \Delta_i \xi_i$ and $r_i = \Delta_{ij} \xi_i$ where Δ_i and Δ_{ij} are the uncertain gain matrices. The uncertainty and interconnection must satisfy the following condition:

$$\|\zeta_i\|^2 \le \|\xi_i\| \text{ and } \|r_i\|^2 \le \|\xi_i\|. \tag{11}$$

Associated with the uncertain systems (7) to (10), we consider a cost function of the form:

$$\int_0^\infty \sum_{i=1}^N \|z_i(t)\| dt \tag{12}$$

The minimax output-feedback controller designed in this paper minimizes the cost in equation (12) subject to the bounds in equation (11) on the local uncertainty and interconnections, $\|\zeta_i\|^2 \le \|\xi_i\|$. In this paper measured output and the controlled variable are the same, i.e., $y_i = z_i$.

The minimax optimal control finds the controller which minimizes the above cost function over all admissible uncertainties which satisfy the following relationship:

$$\inf_{u_i,\, i=1..N} \sup_{\Xi,\Pi} \int_0^\infty \sum_{i=1}^N \|z_i(t)\| dt \le \inf_{\Gamma} \sum_{i=1}^N x_{i0}^T [X_i + \tau_i M_i + \theta_i \overline{M}_i] x_{i0} \tag{13}$$

where $[x_{i0}.....x_{N0}]$ is the initial condition vector, Ξ a set of all admissible uncertainties and Π a set of interconnection inputs, $\Gamma = \{\{\tau_i, \theta_i\}_{i=1}^{N} \in R^{2N}\}$, a set of vectors, and $M_i > 0$ and $\overline{M}_i > 0$ two positive definite symmetrical matrices. Matrices X_i and Y_i are the solutions to the following pair of parameter-dependent coupled algebraic equations [26]:

$$A_i^T Y_i + Y_i A_i + Y_i \overline{B}_{2i} \overline{B}_{2i}^T Y_i - [C_{yi}^T W_i^{-1} C_{yi} - \overline{C}_i^T \overline{C}_i] = 0, \tag{14}$$

$$A_i^T X_i + X_i A_i + \overline{C}_i^T \overline{C}_i - X_i [B_i R_i^{-1} B_i^T - \overline{B}_{2i} \overline{B}_{2i}^T] X_i = 0, \tag{15}$$

where $R_i = \overline{D}_i^T \overline{D}_i$, $W_i = \overline{D}_{yi} \overline{D}_{yi}^T$ and $\overline{\theta}_i = \sum_{n=1, n\neq i}^{N} \theta_n$, $\overline{C}_i = \begin{bmatrix} C_i \\ (\tau_i + \overline{\theta}_i)^{1/2} H_i \end{bmatrix}$,

$\overline{D}_i = \begin{bmatrix} D_i \\ (\tau_i + \overline{\theta}_i)^{1/2} G_i \end{bmatrix}$, $\overline{B}_{2i} = \begin{bmatrix} \tau_i^{-1/2} E_i & \theta_i^{-1/2} L_i \end{bmatrix}$, $D_{yi} = \begin{bmatrix} \tau_i^{-1/2} D_{yi} & 0 \end{bmatrix}$. These solutions are required to satisfy the following conditions:

$\tau_i > 0$, $\theta_i > 0$, $X_i \geq 0$, $Y_i \geq 0$ and $Y_i > X_i$.

Then, the controller is designed using the following equations [26]:

$$\dot{x}_{ci} = \{A_i - [B_i R_i^{-1} B_i^T - \overline{B}_{2i} \overline{B}_{2i}^T] X_i\} x_{ci} + [Y_i - X_i]^{-1} C_{yi}^T W_i^{-1} [y_i(t) - C_{yi} x_{ci}], \tag{16}$$

$$u_i = -R_i^{-1} B_i^T X_i x_{ci}. \tag{17}$$

6. Proposed control algorithm

In this paper, a controller, which can accommodate PV units, ensure dynamic stability and provide the required steady-state voltage is designed. As mentioned earlier, the test system is divided into three subsystems and a controller is designed for each subsystem, the structure of which is shown in Figure 6 and the control design algorithm is implemented in the following steps.

Step 1: Solve the base case power flow and monitor bus voltages.

Step 2: Linearize the complete dynamic system about the equilibrium point. One part of the dynamic system consists of the states of the devices in the subsystem (x_i) and the other the rest of the states (r_i); the matrices A_i and L_i are appropriately chosen from the complete linearized model equations; the other matrices determined in the problem formulations in Section 5 correspond to the control input, measured output and control variable.

Step 3: Increase the generation profile, perform a power flow and check the bus voltage again; if the bus voltages are within the statutory limit (±10% of the nominal voltage), go to the next step, otherwise go to step 10.

Step 4: Obtain the uncertain matrix (E_i) taking the difference between the matrices of subsystem A_i for the nominal and increased generations.

Step 5: Solve the optimization problem using the line search technique for the positive values of τ_i and θ_i with a proper initialization.

Step 6: Substitute the values of τ_i and θ_i and solve the Riccati equations (14) and (15).

Step 7: Design the controller according to equations (16) and (17); if a feasible controller is obtained, go to the next step, otherwise go to step 10.

Step 8: Perform a time-domain simulation and evaluate the controller's performance for the worst-case scenario.

Step 9: If the controller satisfies both the static and dynamic constraints, go to step 3, otherwise go to step 10.

Step 10: Stop and specify the upper level of PV integration.

7. Controller performance evaluation

The performance of the designed robust controller is verified for a meshed system as shown in Figure 4 with three PV generators. Each PV generator consists of a number of PV arrays depending on its rating. A PV array consists of 150 strings connected in parallel, each string is characterized by a rated current of 2.8735 A. Each string is subdivided into 54 modules, characterized by a rated voltage of 43.5 V and connected in series. Thus, the total output voltage of the PV array is 2349 V and output current is 431 A. The value of the DC link capacitor is 5000 μF and the nominal voltage is 1582 V. Solar irradiance is constant at 1.0 kW/m^2. The parameter of the PV system is given in Appendix-I. As, generally, the output voltage of a PV module is low, at first a DC-AC converter is used to convert the output of the PV array into AC which is then stepped up through a transformer. The PV generator is connected to the grid through a low-pass filter and an isolation transformer [23]. A built-in transformer is generally included in the PV system to adapt the VSC AC side terminal voltage to the nominal PCC voltage which is known as an isolation transformer. Next the performance of the designed controller is discussed.

The upper levels of DG penetration using the abovementioned procedure are given in Table I. The output power of each generator is increased simultaneously in order to determine these upper levels. Figure 7 shows the movement of the critical mode with the increment of the PV level for the open loop system. The critical modes are defined as the eigenvalues closest to the imaginary axis with the minimum damping that contribute most to the transient behavior. Critical modes are calculated from eigenvalues and participation factors through modal analysis. From Figure 7 it is clear

that the critical mode moves to the right-half plane and thereby reduces damping which motivates for the design of the robust controller. To assess the performance of the designed controller, the integration level using a properly tuned PI controller [29] is also determined. The PI parameters obtained from the Ziegler Nichols method are K_P=1.6 and K_I=0.4 for P control and K_P=0.6 and K_I=1.25 for Q control. From Table I, it is clear that the designed controller can accommodate more PV units than the conventional PI controller; for example, at bus 50, the integration level can be enhanced by 13.63% using the robust controller. The upper level is determined based on the grid codes [19], i.e., the steady-state voltage remains within ±10% of the nominal voltage, the transient voltage restores within 2 s and the minimum damping of the critical mode is 5%.

<Figure 7>

Figure 7. Movement of the critical mode with the increment of PV level.

To verify the robustness of the designed controller, a number of cases are investigated in which its performances are compared with those of the PI controller under different operating conditions of (i) a sudden change in generation, (ii) a three-phase fault and (iii) a permanent change in the connected load.

Firstly, the controller's performance is verified using a sudden temporary change in generation. Figures 8 and 9 show the real power output and terminal voltage responses of PV_1 for a sudden 20% change in the real power output. It is clear that, although both controllers ensure stable operation, the designed controller provides better performances in terms of damping, oscillations and settling time. Its real power and voltage restore to their pre-fault values within 0.5 s compared with 6 s for the PI controller.

<Figure 8>

Figure 8. Real power of PV_1 for sudden change in generation.

<Figure 9>

Figure 9. Terminal voltage of PV_1 for sudden change in generation.

The performance of the controller is also verified under a three-phase fault. A symmetrical three-phase fault is applied on bus 31 at 1 s and cleared after 0.2 s. Figures 10 and 11 show the output power and terminal voltage responses of the PV using both the proposed robust and conventional controllers from which it is clear that the tuned PI (Ziegler-Nichols method) control produces oscillatory behaviors. However, the robust performance of the designed controller ensures that grid standards and utility requirements are maintained.

<Figure 10>

Figure 10. Real power of PV_3 for three-phase fault.

<Figure 11>

Figure 11. Terminal voltage of PV_3 for three-phase fault.

Finally, the robustness of the controller is tested under different operating conditions. Although the proposed controller is designed for rated operating conditions, it performs well under different loading conditions. This is due to the incorporation of uncertainties in its design and the proposed control algorithm ensuring stability as long as condition (11) holds. Figures 12 and 13 show the PCC voltage and real power output due to the 10% increase in load from which it is clear that the controller stabilizes the system at different equilibrium points.

<Figure 12>

Figure 12. Real power output of PV_1 due to 10% change in load.

<Figure 13>

Figure 13. Voltage of PV_1 due to 10% change in load.

8. Conclusion

A systematic robust control methodology for integrating intermittent renewable generation into existing grids is presented in this paper. Control strategies for PV generators are discussed in detail. The proposed controller ensures stability in the presence of generation uncertainty, interconnection effects and weakly coupled generators with low inertia. The simulation results show that the proposed robust control method can augment the potential penetration of PV units without requiring network reinforcements or violating system operating constraints. Also, the proposed algorithm can be applied to a distribution network with different types of DG units, for example, solar, wind, hydro and CHP. The future aim of this work is to implement the proposed control technique in the laboratory and design coordinate controllers for PV systems.

Acknowledgement

This work was supported by the CSIRO Australia under the Intelligent Grid Flagship Project.

Appendix-I

Base MVA: 10MVA

Bus Data				Line Data			
Bus Number	Load MW	Load MVAr	Base kV	Bus to Bus	Section Resistance (p.u.)	Section Reactance (p.u.)	Section Susceptance (p.u.)
1	0	0	69	3-9	0.00150	0.00125	0.0
2	0	0	69	9-25	0.00424	0.00353	0.0
3	0	0	13.8	9-13	0.00017	0.00014	0.0
4	0	0	13.8	9-12	0.00038	0.00032	0.0
5	0	0	13.8	3-5	0.00075	0.00063	0.0
6	0	0	13.8	3-26	0.00157	0.00131	0.0
7	0	0	13.8	3-6	0.00109	0.00091	0.0
8	6.361	0	13.8	4-15	0.00227	0.00189	0.0
9	0	0	0.48	4-7	0.00000	0.00010	0.0
10	0	0	13.8	7-27	0.00143	0.00119	0.0
11	0.353	0.200	2.4	7-16	0.00275	0.00229	0.0
12	0	0	13.8	10-13	0.00046	0.00039	0.0
13	0	0	13.8	10-12	0.00002	0.00002	0.0
15	0	0	13.8	10-27	0.00110	0.00091	0.0
16	0	0	13.8	4-8	0.00076	0.00092	0.0
17	0.831	0.521	0.48	4-24	0.00118	0.00098	0.0
18	0.831	0.521	0.48	24-31	0.00079	0.00065	0.0
19	2.650	1.502	2.4	24-32	0.00112	0.00093	0.0
20	2.650	1.502	2.4	28-38	0.03039	0.02929	0.0
21	0.421	0.283	0.48	33-28	0.03813	0.02450	0.0
22	0.084	0.057	0.48	29-38	0.04012	0.03866	0.0
23	0.084	0.057	0.48	34-29	0.03813	0.02450	0.0
24	0	0	0.48	38-30	0.06079	0.05858	0.0
25	0	0	13.8	35-30	0.03813	0.02450	0.0
26	0	0	13.8	22-17	0.03813	0.02450	0.0
27	0	0	13.8	23-18	0.03813	0.02450	0.0
28	0.578	0.351	0.48	50-3	0.00122	0.00243	0.0
29	0.703	0.426	0.48	100-1	0.00139	0.00296	0.00480
30	0.563	0.349	0.48	100-2	0.00139	0.00296	0.00480
31	0	0	13.8	28-41	0.03429	0.02094	0.0
37	0.663	0.394	0.48				
38	0	0	0.48				
39	1.237	0.701	4.16				
41	0.150	0.049	0.48				
49	0.963	0.520	0.48				

50	0	0	13.8				
51	0.478	0.307	0.48				
100	0	0	69				

Bus to Bus	Resistance (p.u.)	Reactance (p.u.)	kVA	%Z	X/R ratio	kV Ratio
1-3	0.00313	0.05324	15000	8.00	17.00	69/13.8
2-4	0.00313	0.05324	15000	8.00	17.00	69/13.8
5-39	0.04314	0.34514	1725	6.00	8.00	13.8/4.16
6-11	0.05575	0.36240	1500	5.50	6.50	13.8/2.4
12-17	0.06843	0.44477	1500	6.75	6.50	13.8/0.48
13-18	0.05829	0.37888	1500	5.75	6.50	13.8/0.48
6-19	0.01218	0.14616	3750	5.50	12.00	13.8/2.4
15-20	0.01218	0.14616	3750	5.50	12.00	13.8/2.4
16-21	0.15036	0.75178	750	5.75	5.00	13.8/0.48
25-28	0.05829	0.37888	1500	5.75	6.50	13.8/0.48
26-29	0.05829	0.37888	1500	5.75	6.50	13.8/0.48
27-30	0.05829	0.37888	1500	5.75	6.50	13.8/0.48
31-36	0.02289	0.22886	2500	5.75	10.00	13.8/2.4
32-37	0.10286	0.56573	1000	5.75	5.50	13.8/0.48
5-49	0.05918	0.35510	1250	4.50	6.00	13.8/0.48
50-51	0.06391	0.37797	1500	5.75	5.91	13.8/0.48

PV System Data			
Number of PV cells per module	54	Voltage temperature coefficient	-0.1 V/K
Number of parallel modules in each row	150	Current temperature coefficient	0.003 A/K
Module current rating	2.8735 A	Diode ideality factor	1.3
Module voltage rating	43.5 V	VSC switching frequency	3060 Hz
DC-link capacitor	5000 μF	On-resistance of VSC valves	1 mΩ
Inductance of filter	100 μH	Capacitance of filter	369 μF

References

[1] Dufo-López R.,. Zubi G, Fracastoro G. V. Tecno-economic assessment of an off-grid PV-powered community kitchen for developing regions. Applied Energy, 2012; 91(1):255-262.

[2] Matallanas E., Castillo-Cagigal M., Gutiérrez A., Monasterio-Huelin F., Caamaño-

Martín E, Masa D., Jiménez-Leube J. Neural network controller for Active Demand-Side Management with PV energy in the residential sector. Applied Energy, 2012; 91(1):90-97.

[3] Dufo-López R., Bernal-Agustín J. L., Yusta-Loyo J. M., Domínguez-Navarro J. A., Ramírez-Rosado I. J., Lujano J., Aso I. Multi-objective optimization minimizing cost and life cycle emissions of stand-alone PV-wind-diesel systems with batteries storage. Applied Energy 2011; 88(11):4033-4041.

[4] Zejli D., Ouammi A., Sacile R., Dagdougui H., Elmidaoui A. An optimization model for a mechanical vapor compression desalination plant driven by a wind/PV hybrid system. Applied Energy 2011; 88(11):4042-4054.

[5] Wei Zhou W., Lou C., Li Z., Lu L., Yang H. Current status of research on optimum sizing of stand-alone hybrid solar-wind power generation systems. Applied Energy 2010; 87(2):380-389.

[6] O'Gorman R., Redfern M. A. Voltage control problem on modern distribution system. IEEE Power and Energy Systems General Meeting 2004: 662-667.

[7] Kalaitzakis K.C., Vachtsevanos G.J. On the control and stability of grid connected photovoltaic sources. IEEE Trans. on Energy Conversion 1987; EC-2: 556-562.

[8] Xin H., Gan D., Huang Z., Zhuang K., Cao L. Applications of stability-constrained optimal power flow in the East China system. IEEE Trans. on Power Systems 2010; 25: 1423-1433.

[9] Tsikalakis A., Hatziargyriou N. On centralized control for optimizing microgrids operation. IEEE Trans. on Energy Conversion 2008; 23: 241-248.

[10] Kakimoto N., Piao Q.Y., Ito H. Voltage control of photovoltaic generator in combination with series reactor. IEEE Trans. on Sustainable Energy 2011; 2: 374-

382.

[11] Datta M., Senjyu T., Yona A., Funabashi T., Kim CH. A frequency control approach by photovoltaic generator in a PV–Diesel hybrid power system. IEEE Trans. on Energy Conversion 2011; 26: 559-571.

[12] Kakimoto N., Takayama S., Satoh H., Nakamura K. Power modulation of photovoltaic generators for frequency control of power systems. IEEE Trans. on Energy Conversion 2009; 24: 943-949.

[13] Xin H., Qu Z., Seuss J., Maknouninejad A. A self-organizing strategy for power flow control of photovoltaic generators in a distribution network. IEEE Trans. on Power Systems 2011; 26: 1462-1473.

[14] Kwon J.M., Kwon B.H., Nam K.H. Three-phase photovoltaic system with three-level boosting MPPT control. IEEE Trans. on Power Electronics 2008; 23: 2319-2327.

[15] Diaz G., Gonzaalez-Moran C., Gomez-Aleixandre J. et al. Complex-valued state matrices for simple representation of large autonomous microgrids supplied by PQ and V f generation. IEEE Trans. on Power Systems 2009; 24: 1720-1730.

[16] Kaneko T., Uehara A., Senjyu T., Yona A., Urasaki N. An integrated control method for a wind farm to reduce frequency deviations in a small power system. Applied Energy 2011; 88(4):1049-1058.

[17] Katiraei F., Iravani M. Power management strategies for a microgrid with multiple distributed generation units. IEEE Trans. on Power Systems 2006; 21: 1821-1831.

[18] Delfino F., Procopio R., Rossi M., Ronda G. Integration of large-scale photovoltaic systems into the distributed grids: a P-Q chart approach to access reactive support capability. IET Renewable Power Generation 2010; 4: 329-340.

[19] Hossain M.J., Pota H.R., Ugrinovskii V.A., Ramos R.A. Simultaneous STATCOM and pitch angle control for improved LVRT capability of fixed-speed wind turbines. IEEE Trans. on Sustainable Energy 2010; 1: 142-151.

[20] Hossain M.J., Pota H.R., Ugrinovskii V.A., Ramos R.A. Voltage mode stabilization in power systems with dynamic load. International Journal of Electrical Power and Energy Systems 2010; 32: 911-920.

[21] Yun Tiam Tan, Kirschen D.S., Jenkins N. A model of PV generation suitable for stability analysis. IEEE Trans. on Energy Conversion 2004; 19: 748-755.

[22] Nosrat A., Pearce J. M. Dispatch strategy and model for hybrid photovoltaic and tri-generation power systems. Applied Energy 2011; 88(9): 3270-3276.

[23] Yazdani A., Rita Di Fazio A., Ghoddami H., Russo M., Kazerani M., Jatskevich J., Strunz K., Leva S., Martinez J.A. Modeling guidelines and a benchmark for power system simulation studies of three-phase single-stage photovoltaic systems. IEEE Trans. on Power Delivery 2011; 26: 1247-1264.

[24] Rodriguez C., Amaratunga G.A.J. Dynamic stability of grid connected photovoltaic systems. IEEE Power Engineering Society General Meeting 2004: 2193-2199.

[25] IEEE Standard for Interconnecting Distributed Resources with Electric Power Systems. IEEE std. 1547-2003, 2003.

[26] Hossain M.J., Pota H.R., Kumble C. Decentralized robust static synchronous compensator control to augment dynamic transfer capability. Journal of Renewable and Sustainable Energy 2010; 2: 022701(1)-(17).

[27] Hossain M.J., Pota H.R., Ugrinovskii V.A., Ramos R.A. Decentralized control to augment LVRT capability of wind generators with STATCOM/ESS. IEEE Power and Energy Society General Meeting 2010: 1-8.

[28] Li L., Ugrinovskii V.A., Orsi R. Decentralized robust control of uncertain Markov jump parameter systems via output feedback. Automatica 2007; 43: 1922-1944.

[29] Mallesham G., Mishra S., Jha A.N. Maiden application of Ziegler Nichols method to AGC of distributed generation system. IEEE/PES Power Systems Conference and Exposition 2009: 1-7.

List of figures

Tables

TABLE I: PENETRATION LEVELS (MW)

Control	Bus 4 PV_1	Bus 50 PV_2	Bus 39 PV_3
PI	15.25	14.85	18.15
Robust	16.75	17.25	19.65

Figures

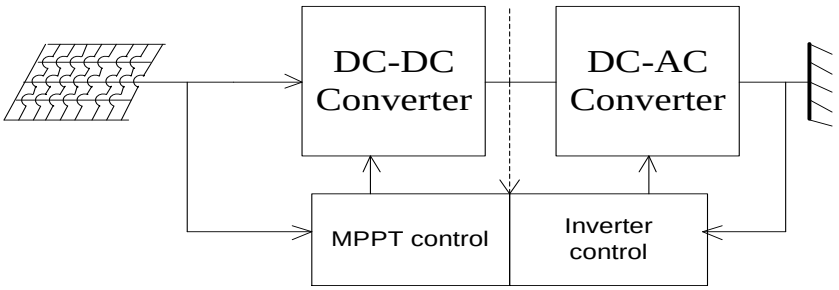

Figure 1. PV system connected to grid

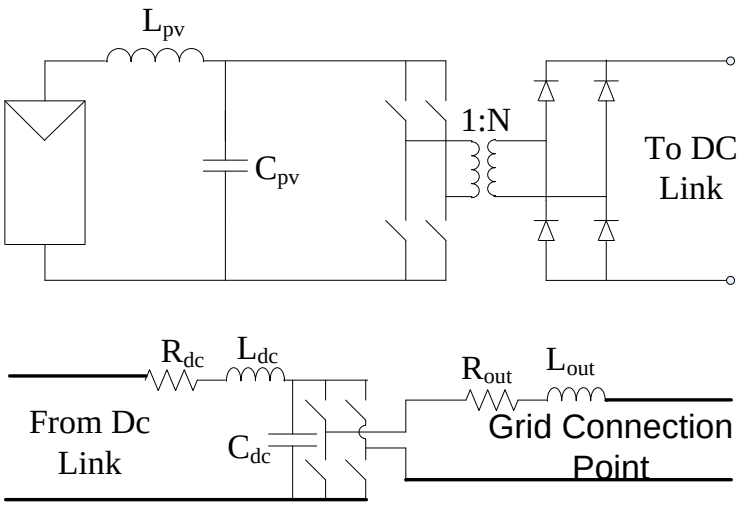

Figure 2. Equivalent model of grid-connected PV system.

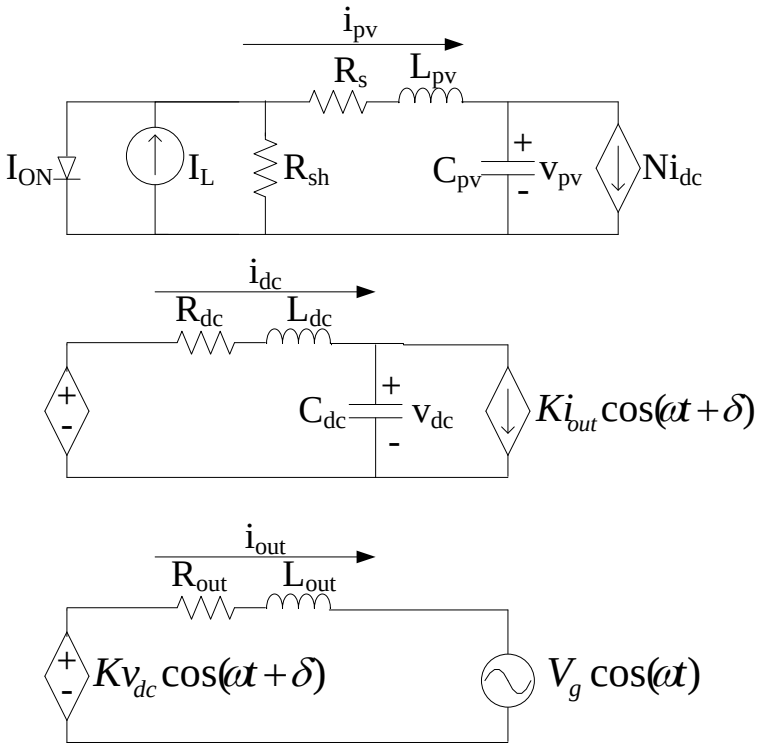

Figure 3. Equivalent circuit diagram of grid-connected PV system

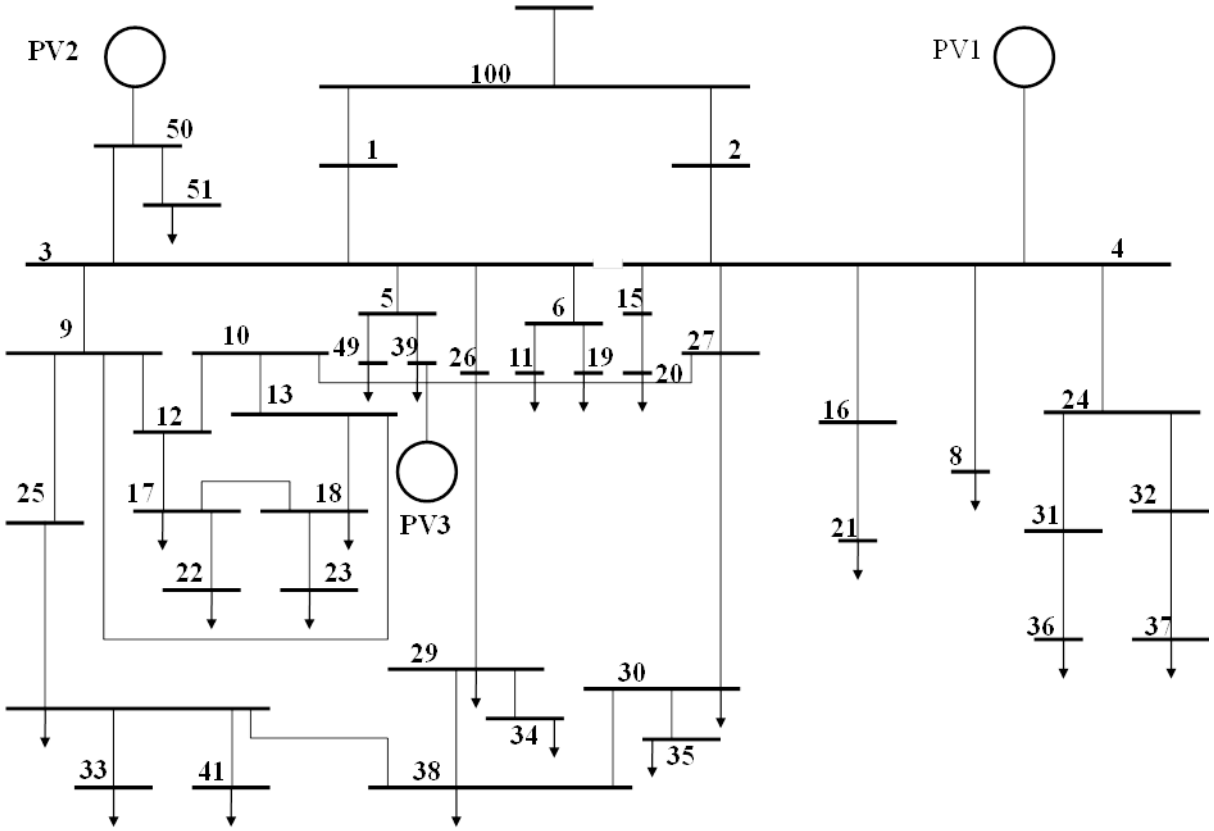

Figure 4. Single-line diagram of 43-bus test distribution system

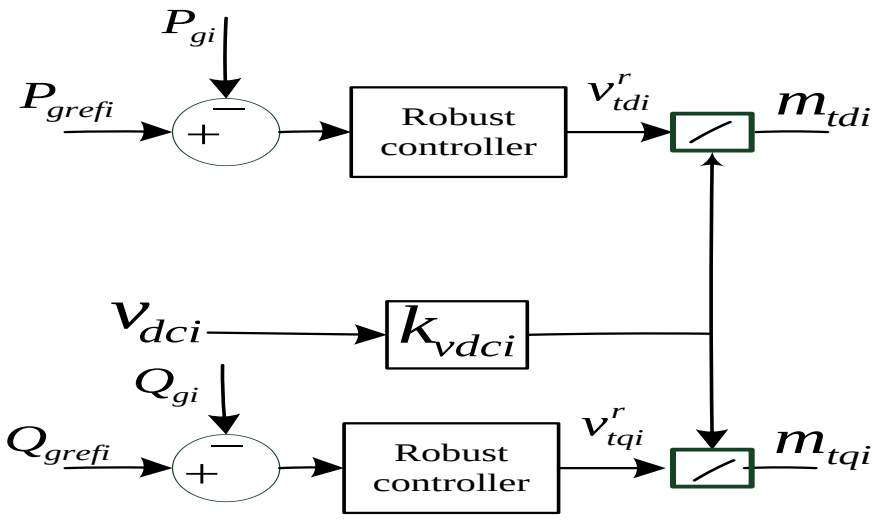

Figure 5. Control strategy for PV

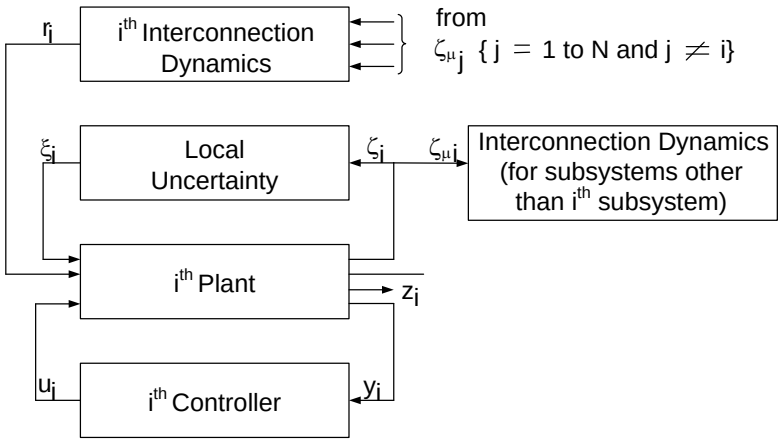

Figure 6. Block diagram of decentralized control

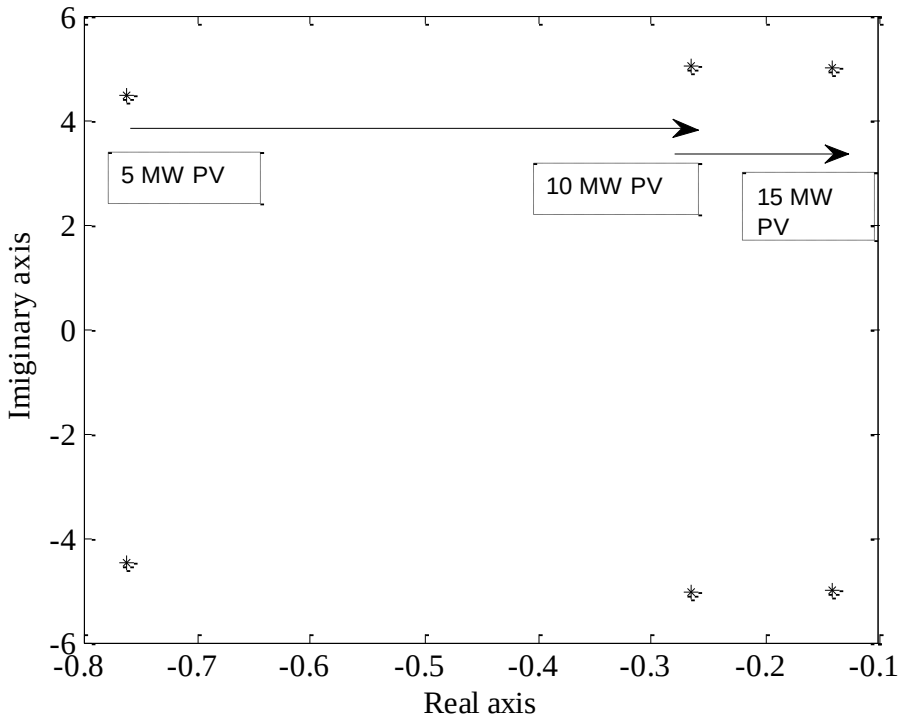

Figure 7. Movement of the critical mode with the increment of PV level

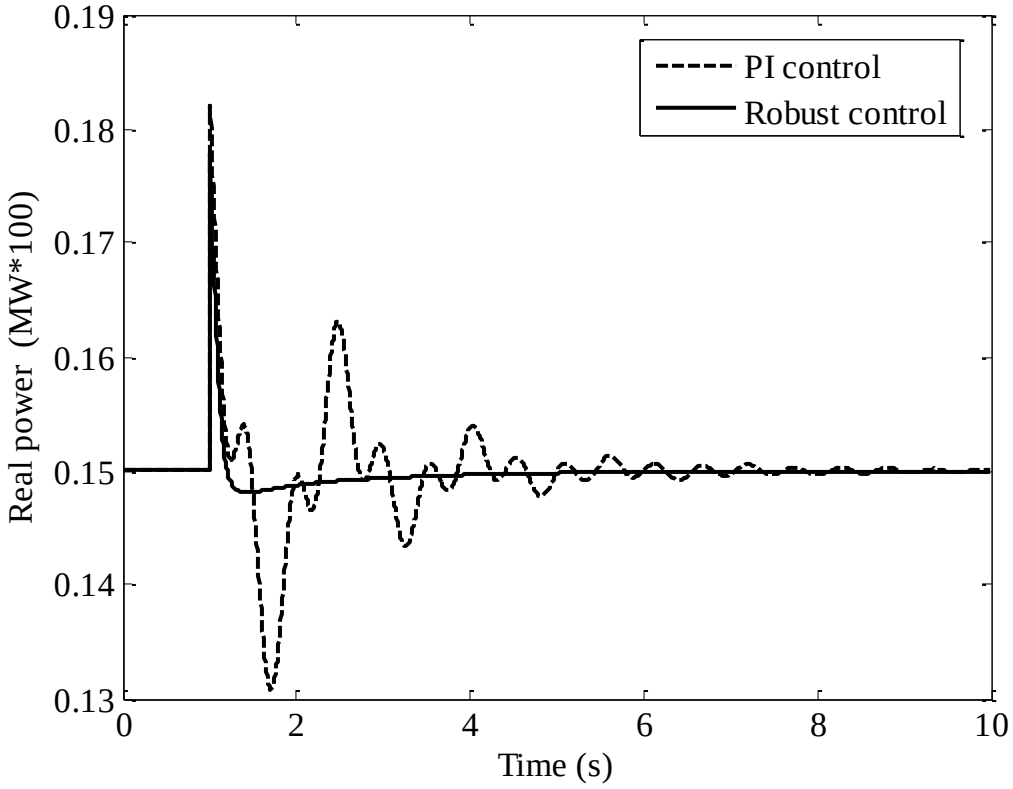

Figure 8. Real power of PV_1 for sudden change in generation.

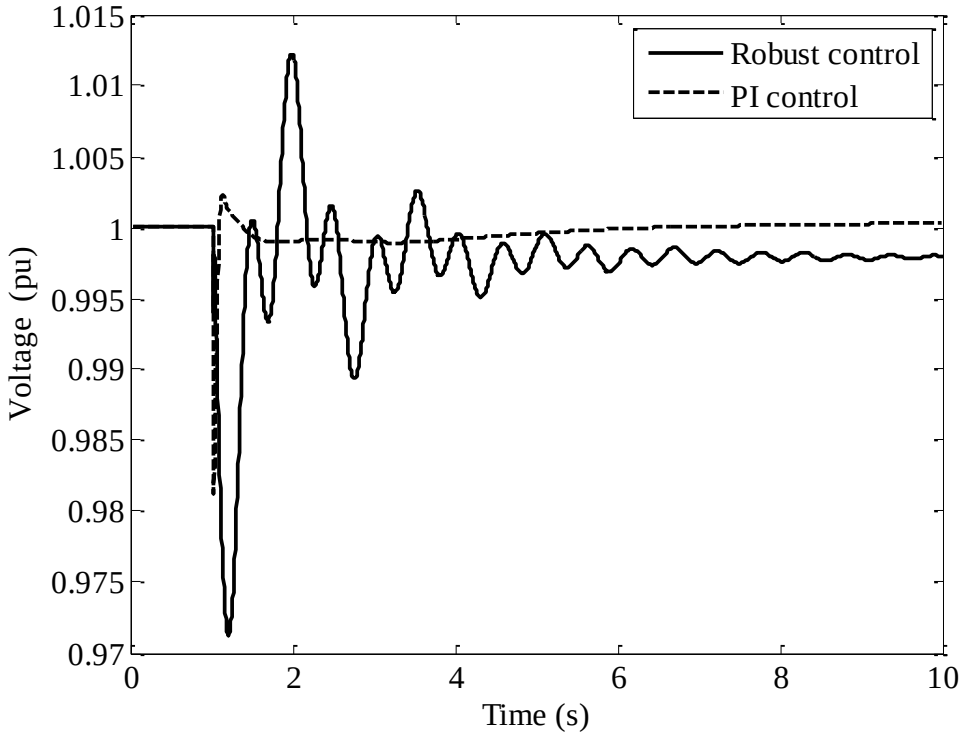

Figure 9. Terminal voltage of PV_1 for sudden change in generation.

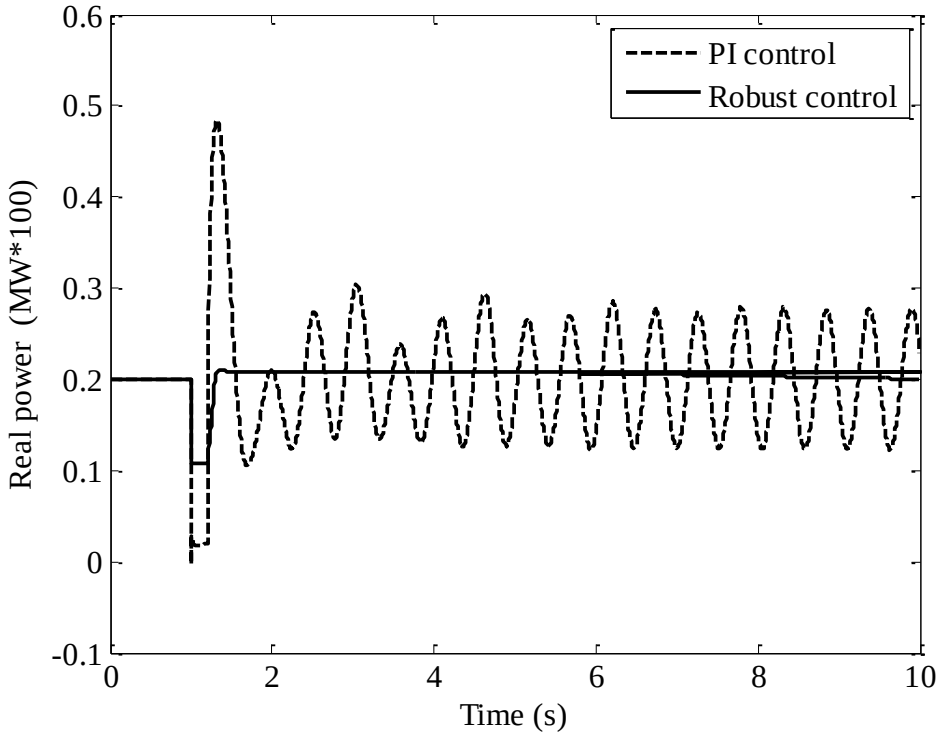

Figure 10. Real power of PV_3 for three-phase fault.

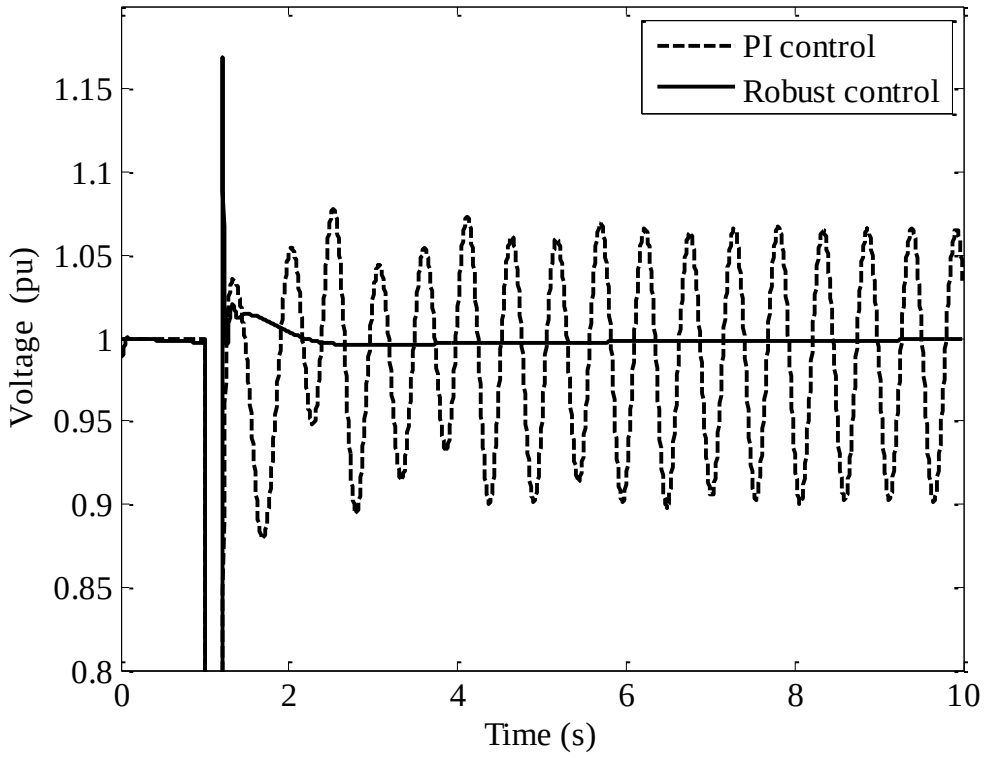

Figure 11. Terminal voltage of PV_3 for three-phase fault.

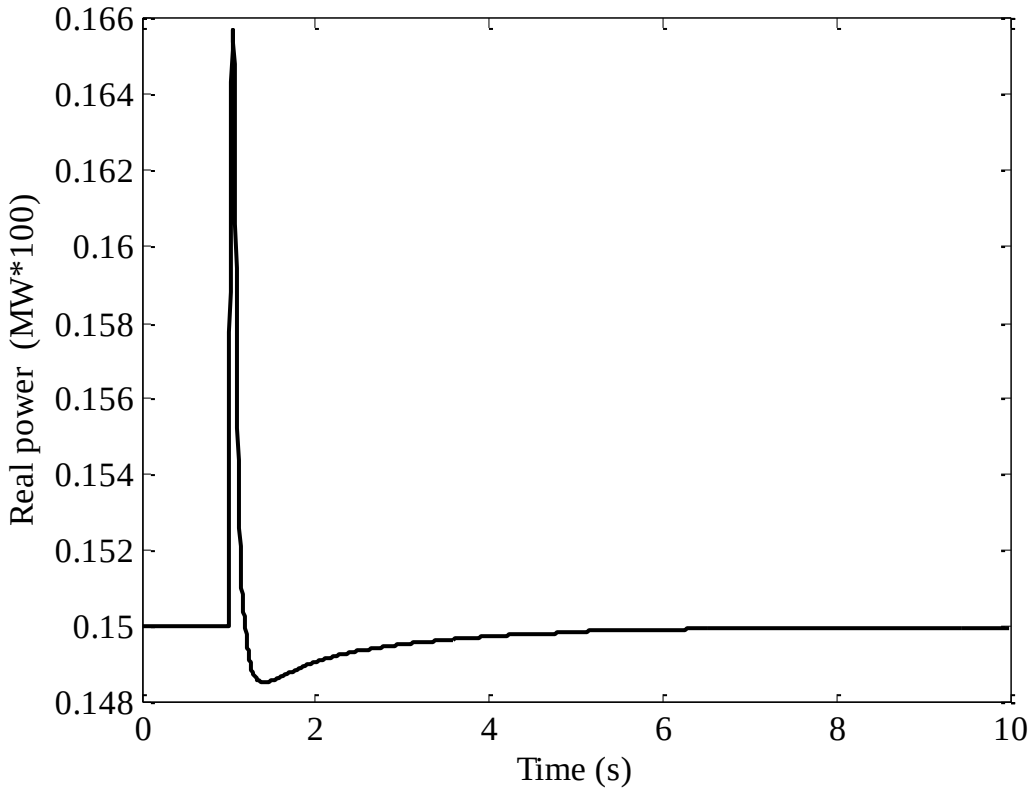

Figure 12. Real power output of PV_1 due to 10% change in load.

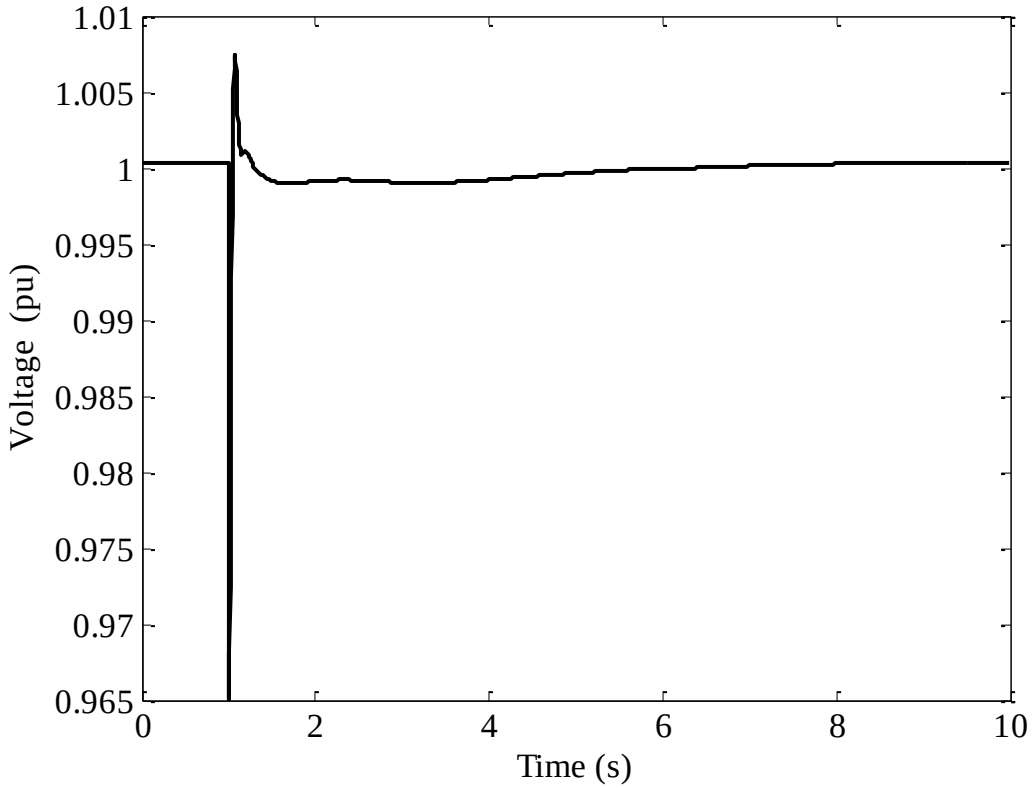

Figure 13. Voltage output of PV_1 due to 10% change in load.